European Journal of Radiology 114 (2019) 152–159

Contents lists available at ScienceDirect

European Journal of Radiology

journal homepage: www.elsevier.com/locate/ejrad

Noninvasive assessment of H3 K27M mutational status in diffuse midline gliomas by using apparent diffusion coefficient measurements

Hong Chen[a,b,1], Wanming Hu[c,1], Haoqiang He[a], Yuanzhong Yang[c], Ge Wen[b,*], Xiaofei Lv[a,*]

[a] Department of Medical Imaging, State Key Laboratory of Oncology in South China, Collaborative Innovation Center for Cancer Medicine, Sun Yat-Sen University Cancer Center, Guangzhou, 510060, PR China

[b] Department of Medical Imaging Center, Nanfang Hospital, Southern Medical University, Guangzhou, PR China

[c] Department of Pathology, State Key Laboratory of Oncology in South China, Collaborative Innovation Center for Cancer Medicine, Sun Yat-Sen University Cancer Center, Guangzhou, 510060, PR China

ARTICLE INFO

Keywords:
Conventional MRI
Diffusion-weighted imaging
H3 K27M-mutant

ABSTRACT

Purpose: H3 K27M-mutant diffuse midline gliomas are associated with worse prognosis than H3 K27M wild-type gliomas. In the present study, we sought to evaluate the conventional magnetic resonance imaging (cMRI) of H3 K27M-mutant glioma and examine whether diffusion-weighted imaging (DWI) derived apparent diffusion coefficient (ADC) could noninvasively predict H3 K27M mutational status in brain diffuse midline gliomas.

Materials and methods: The institutional review board approved this study and waived the requirement for informed consent. Thirty-eight patients with brain diffuse midline gliomas were retrospectively reviewed. The parameters of preoperative cMRI were evaluated. The minimal ADC, peritumoral ADC, ratio of minimal ADC, and ratio of peritumoral ADC were measured, and significant differences between the two groups were identified by logistic regression analysis adjusted for age and tumor location. Receiver operating characteristic curves and logistic regression analysis adjusted for age and tumor location were used to assess the diagnostic performances of the minimal ADC, peritumoral ADC, ratio of minimal ADC, and ratio of peritumoral ADC.

Results: H3 K27M-mutant gliomas in different locations have diverse imaging characteristics. Minimal ADC, peritumoral ADC, ratio of minimal ADC, and ratio of peritumoral ADC values were significantly lower in the H3 K27M-mutant gliomas than in the wild-type gliomas ($P < 0.05$). The combination of ratio of minimal ADC and ratio of peritumoral ADC provided the largest area under the curve (AUC) of 0.872 in defining H3 K27M-mutational status.

Conclusions: The combination of ratio of minimal ADC and ratio of peritumoral ADC can noninvasively detect the H3 K27M mutational status in brain diffuse midline gliomas.

1. Introduction

H3 K27M-mutant diffuse midline glioma is a new diagnosis entity classified by the revised 2016 World Health Organization (WHO) Classification of Tumors of the central nervous system (CNS) [1]. These diffuse midline gliomas contain mutations in genes of H3F3A and HIST1H3B encoding the histone H3.3 variant H3.1, resulting in a p.Lys27Met amino acid substitution [2,3]. In contrast, hemispheric tumors contain a p.Gly34Arg alteration in the H3F3A gene [4]. Recent studies have demonstrated that diffuse midline gliomas with histone H3 K27M mutations drive aggressive clinical behavior and have a poor prognosis [5,6], even though mitosis, microvascular proliferation or necrosis are not found in biopsies [7]. The H3 K27M mutations primarily occur in children, but they can also be observed in adults [5,8]. These gliomas are commonly located in the midline structure, such as the thalamus, brainstem, cerebellum, and spinal cord [9]. Because of the deep location of the midline gliomas, surgical resection and stereotactic biopsy are difficult to conduct. Most of the cases are diagnosed on the basis of imaging findings, resulting in a limited preoperative strategies available to study. Therefore, a noninvasive method by using imaging findings to detect the H3 K27M mutation is critical to develop a proper therapeutic plan.

Diffusion-weighted imaging (DWI) has been investigated for the determination of gliomas grading and for detecting the genetic features of gliomas [10–12]. DWI is a technique that reflects tumor cellularity and lesion aggressiveness, wherein low apparent diffusion coefficient

* Corresponding authors.
E-mail addresses: wenge67@aliyun.com (G. Wen), lvxf@sysucc.org.cn (X. Lv).

[1] Co-first authorship: These authors contributed equally to this work.

https://doi.org/10.1016/j.ejrad.2019.03.006
Received 28 October 2018; Received in revised form 6 March 2019; Accepted 13 March 2019

(ADC) values are generally associated with increased tumor cellularity [13]. To date, ADC values have been demonstrated to have potential for reflecting the microenvironment heterogeneity and may distinguish the isocitrate dehydrogenase (IDH) gene status of the gliomas [14]. Conventional magnetic resonance imaging (cMRI) findings were commonly used to evaluate features of brain tumors [15]. A previous study showed that combining DWI and cMRI allows more accurate prediction of gene status [16]. However, to our knowledge, there are only few reports using DWI techniques derived ADC to distinguish H3 K27M mutational status in brain midline gliomas in both children and adults.

Therefore, we retrospectively analyzed the clinical, pathological, cMRI, and DWI imaging features of brain diffuse midline gliomas in children and adults. The purpose of our study was to noninvasively identify MRI markers predictive of H3 K27 M mutational status in diffuse midline tumors.

2. Materials and methods

2.1. Patient cohort

We retrospectively searched the database of our hospital (Sun Yat-sen University Cancer Center) for CNS tumors located in the midline structure, including the pineal region, corpus callosum, thalamus, hypothalamus, midbrain, pons, cerebellum, vermis/fourth ventricle, and spinal cord. Patients who had not received chemotherapy, stereotactic biopsy, or surgery before MR examination were included. All patients underwent surgical resection or stereotactic biopsy within one month of MR examination. The exclusion criteria were as follows: (a) there were no tumor tissue samples available in our hospital; (b) the paraffin-embedded tumor tissues were insufficient to test the gene status; (c) patient without an MR examination before surgery; (d) patient who had a history of surgery outside our hospital before MR examination; (e) the tumors were pilocytic astrocytoma of WHO grade I; and (f) the tumors were located in the spinal cord. Finally, 38 patients with diffuse midline gliomas, including 19 patients with H3 K27M-mutant and 19 patients with wild-type tumors, who were treated from January 2011 to June 2018 were retrospectively evaluated (Fig. 1).

2.2. Histology and gene analysis

Thirty-seven of the 38 patients underwent surgery, and 1 patient underwent stereotactic biopsy. All available surgical or biopsy tissues were examined, and all cases were assigned a diagnosis and grade. Hematoxylin and eosin (H&E)-stained sections were reviewed for diagnostic evaluation and morphological variation. The histone H3 K27 M status was identified according to the 2016 WHO classifications of CNS tumors. Immunohistochemistry was performed with the formalin-fixed paraffin-embedded tumor tissue using the histone H3 mutant-specific antibody (ABE419, EMD Millipore, Billerica, MA, USA). This antibody showed a strong nuclear staining for the H3 K27 M genotype [17]. Histone H3 K27 M immunostaining was performed in a Ventana Benchmark XT autostainer by using the Cell Conditioning 1 antigen retrieval buffer for 30 min at 95 °C, followed by incubation with a primary antibody at 1:500 dilution for 32 min, and then detection by the Ventana UltraView Universal DAB detection kit [18].

2.3. MR examinations

All MR images were obtained on either 1.5 T or 3 T clinical scanners. CMRI was performed using the following protocol for all the patients: axial T2-weighted imaging (TR/TE = 4,000–9,638 ms/92.4–119 ms), axial fluid attenuated inversion recovery (FLAIR) imaging (TR/TE/TI = 8,000–9,000 ms/86.8–132.1 ms/2,371.7–2,474.7 ms), and T1-weighted imaging (TR/TE = 350–2,000 ms/6.9–25.2 ms) without and with intravenous gadolinium, slice thickness = 5 mm, and spacing = 1 mm. The parameters of DWI were as follows: TE = 64–93 ms, TR = 3000–6000 ms, NEX = 1–4, Matrix = 128 × 128–192 × 192 mm^2, FOV = 23 × 23–27 × 27 mm^2. All DWI acquisitions included the values of $b = 0$ and $b = 1{,}000\ s/mm^2$ with diffusion gradients encoded in the 3 orthogonal directions. The ADC map was calculated using the software incorporated into the MR imaging unit.

2.4. Qualitative MRI characteristics

MR images were reviewed using a picture archiving and communication system (PACS). The following MR parameters were evaluated for qualitative analysis: (a) tumor location, recorded as the main site occupied by the tumor; (b) multifocality, defined as two or more occupied points connected by direct transmission pathways; (c) lesion size, measured as the maximum diameter on axial unenhanced T2-weighted MR images; (d) tumor shape, evaluated on axial and sagittal MR images and described as round, oval, or irregular; (e) lesion composition, defined as solid, or cystic (if the maximum diameter of the cystic component was greater than 1 cm); (f) hemorrhage, defined as high signal intensity on T1-weighted images, low signal intensity on T2-weighted images, and without enhancement; (g) tumor margins, defined as sharp or blurred; (h) edema, defined as a region containing non-enhanced and higher signal area outside the tumor parenchyma on T2WI and FLAIR sequences; and (i) enhancement pattern, classified as intratumoral rim enhancement, heterogeneous enhancement, marginal enhancement, no or minimal enhancement.

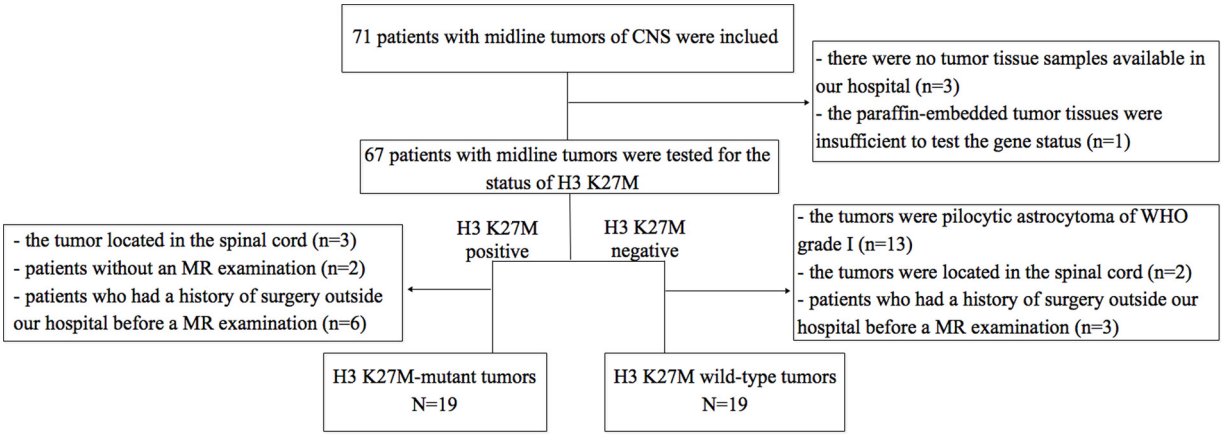

Fig. 1. Flowcharts of inclusion and exclusion criteria.

Table 1
Demographics and clinical characteristics of H3 K27M mutant gliomas.

Variable	H3 K27M-mutant (n = 19)	H3 K27 M wild-type (n = 19)	*P* Value
Clinical Findings			
Age at diagnosis(y)			
Mean ± SD	27.0 ± 14.7	41.8 ± 18.4	0.009*
≤18y	6	2	0.232
> 18y	13	17	
Sex			0.495
Male	11	14	
Female	8	5	
Symptoms			> 0.999
Thalamic dysfunction	10	11	
Intracranial hypertension	7	6	
cerebellum dysfunction	1	1	
Optic nerve-related symptoms	1	1	
Histology			> 0.999
Diffuse astrocytoma	3	3	
Oligodendroglioma	1	2	
Anaplastic astrocytoma	4	5	
Anaplastic oligodendroglioma	1	0	
Glioblastoma	10	9	
Histopathological Grade			> 0.999
II	4	5	
III	5	5	
IV	10	9	
Location			0.727
Thalamus	12	9	
Midbrain	1	3	
Pons	2	1	
Corpus callosum	2	4	
Cerebellum	1	1	
Hypothalamus	1	0	
Medulla oblongata	0	1	

2.5. Quantitative MRI measurements

DWI sequences were missing in two cases, and had invalid parameters in five cases. Overall, ADC values were available in 31 cases in total. The ROIs were drawn by a neuroradiology fellow and confirmed by a neuroradiologist (with 3 and 10 years of experience, respectively, in neurology MR imaging interpretation). Both observers were blinded to the clinical and histopathological results and H3 K27 M status. The final decisions were made by consensus for discordant cases. The ROIs were measured in the ADC grayscale map manually. The size of each ROI was about 25-40 mm^2. The minimal ADC was measured by placing at least five regions of interests (ROIs) in the lowest signal intensity ADC grayscale map within the tumor solid area. Necrosis, cysts, calcification, vasculature, or hemorrhage were avoided as much as possible. Finally, the lowest ADC value among the several ROIs was chosen as the result, which is speculated to represent higher cell density [19]. The ROI of the peritumoral region was drawn in the edema area. If the edema area could not be observed, the ROI was artificially placed in the peritumoral region less than 1 cm adjacent to the tumor area. The method to draw ROI from the internal capsule was to place a ROI in the apparently normal posterior limb of internal capsule, the ROI was centered in the structure of the posterior limb of internal capsule, avoiding border areas. To normalize the ADC values, the apparently normal posterior limb of the internal capsule was measured as the control. The ratio of minimal ADC, ratio of peritumoral ADC were equal to the minimal ADC and peritumoral ADC divided by the normal ADC [20,21].

2.6. Statistical analysis

The Kolmogorov-Smirnov test was performed to analyze whether the continuous variables were normally distributed. All quantitative variables are presented as mean ± SD. Continuous variables were compared using the Student t-test. Fisher's exact tests were performed for categorical variables. The significant differences of minimal ADC, peritumoral ADC, ratio of minimal ADC, and ratio of peritumoral ADC between the two groups were identified by logistic regression analysis adjusted for age and tumor location [22]. Receiver operating characteristic curves and logistic regression analysis adjusted for age and tumor location were used to assess the diagnostic performances of the minimal ADC, peritumoral ADC, ratio of minimal ADC, and ratio of peritumoral ADC. By using the receiver operating characteristic curve (ROC) analysis, the best cut-off for quantitative variables corresponding to maximal Youden index (YI) was determined. Sensitivity, specificity, and area under the curve (AUC) were presented with 95% confidence intervals. All statistical analyses were performed using the SPSS software version 23.0 (IBM Corp.). A *P* value of less than 0.05 (two tailed) was considered as statistically significant.

3. Results

3.1. Clinical and pathological findings

We found nineteen (50%) H3 K27M-mutant cases and 19 (50%) H3 K27 M wild-type cases in this study. H3 K27M-mutant patients were 15 years younger than the wild-type patients (27.0 ± 14.7 vs 41.8 ± 18.4 years, $P = 0.009$). 6 patients were under 18 years old in the H3 K27M-mutant group, 2 patients were under 18 year old in the H3 K27M wild-type group. There was no significant difference in gender distribution between the two groups. Thalamic dysfunction was the most common complaint for patients in both groups, followed by intracranial hypertension, cerebellum dysfunction, and optic nerve-related symptoms. The most frequent locations of the H3 K27M-mutant gliomas were the thalamus (63.2%), midbrain (5.3%), pons (10.5%), corpus callosum (10.5%), cerebellum (5.3%), and hypothalamus (5.3%). Histopathological review revealed that among the H3 K27M-mutant gliomas, glioblastoma (WHO grade IV) was found in 10 cases, diffuse astrocytoma (grade II) in 3 cases, oligodendroglioma (grade II) in 1 case, anaplastic astrocytoma (grade III) in 4 cases, and anaplastic oligodendroglioma (grade III) in 1 case. Overall, the histology and WHO histopathological grade did not vary significantly according to the H3 K27M mutational status of the tumors. (Table 1)

3.2. MRI characteristics

Among the diffuse gliomas located in the thalamus, 10 of 12 H3 K27M-mutant gliomas exhibited a round or oval shape, whereas 6 of the 9 H3 K27 M wild-type gliomas exhibited a round or oval shape; edema was observed in 3 of 12 cases with H3 K27M-mutant gliomas, and in 3 of 9 H3 K27M wild-type gliomas; multifocality was found in 4 of 12 H3 K27M-mutant gliomas and in 7 of 9 H3 K27M wild-type gliomas; the H3 K27M-mutant gliomas displayed intratumoral rim enhancement in 4 of 12 cases, whereas 1 of 9 H3 K27M wild-type gliomas displayed intratumoral rim enhancement. It seems that H3 K27M-mutant gliomas in the thalamus tended to be absence of multifocality and displayed intratumoral rim enhancement more frequently than the H3 K27M wild-type group, however, the small sample size could lead to bias. No differences in maximum diameter, shape, multifocality, composition, hemorrhage, tumor margins, edema, or enhancement pattern were observed between the tumor groups in the brainstem, corpus callosum, or other locations. (Table 2, Figs. 2–4).

The minimal ADC ($\times 10^{-3}\,mm^2/s$) values (H3 K27M-mutant = 0.734 ± 0.120, wild-type = 0.864 ± 0.112, $P = 0.020$), peritumoral ADC values (H3 K27M-mutant = 0.937 ± 0.156, wild-type = 1.161 ± 0.240, $P = 0.018$), ratio of minimal ADC (H3 K27M-mutant = 0.972 ± 0.165, wild type = 1.180 ± 0.162, $P = 0.018$), and ratio of peritumoral ADC (H3 K27M-mutant = 1.240 ± 0.232, wild type =

Table 2
Conventional MRI characteristics of H3 K27M-mutant and H3 K27M wild-type gliomas in different locations.

Conventional MRI features	Thalamus		Brainstem		Corpus callosum		Others	
	H3 K27M (n = 12)	H3 wild-type (n = 9)	H3 K27M (n = 3)	H3 wild-type (n = 5)	H3 K27M (n = 2)	H3 wild-type (n = 3)	H3 K27M (n = 2)	H3 wild-type (n = 2)
age at diagnosis (y)	24.7 ± 13.1	46.8 ± 20.0	25.3 ± 19.1	41.0 ± 13.2	29.0 ± 12.7	39.7 ± 15.7	41.5 ± 24.7	24.5 ± 29.0
Size(mm)	48.9 ± 12.2	50.4 ± 13.9	51.3 ± 10.1	14.5 ± 14.5	49.7 ± 15.6	70.7 ± 8.3	35.5 ± 3.5	21.5 ± 0.7
Shape								
Round or oval	10	6	1	3	0	0	1	0
Irregular	2	3	2	2	2	3	1	2
Multifocality								
Yes	4	7	2	2	2	3	1	1
No	8	2	1	3	0	0	1	1
Composition								
Solid	2	4	0	2	1	2	1	0
Cystic	10	5	3	3	1	1	1	2
Hemorrhage								
Yes	3	3	0	2	0	1	0	0
No	9	6	3	3	2	2	2	2
Tumor margin								
Sharp	8	6	0	3	0	1	0	1
Blurred	4	3	3	2	2	2	2	1
Edema								
Yes	3	1	1	3	2	3	1	1
No	9	8	2	2	0	0	1	1
Enhancement Pattern								
Intratumoral rim enhancement	4	1	0	2	1	0	1	0
Marginal	0	1	1	3	0	0	0	1
Heterogenous	4	7	0	0	0	0	0	0
No or minimal enhancement	4	0	2	0	1	3	1	1

1.582 ± 0.320, $P = 0.013$) were significantly lower in the H3 K27M-mutant group than the H3 K27M wild-type group. There was no statistically significant difference in ADC in the internal capsule between the 2 tumor groups (Table 3, Fig. 5).

3.3. ROC and logistic regression analysis

On the basis of ROC analysis, the optimal cut-off points for sensitivity and specificity for predicting H3 K27 M mutation were 0.728 for minimal ADC ($\times 10^{-3}$ mm^2/s), 1.004 for peritumoral ADC, 0.982 for ratio of minimal ADC and 1.248 for ratio of peritumoral ADC. The AUCs of minimal ADC, peritumoral ADC, ratio of minimal ADC and ratio of peritumoral ADC were 0.842, 0.806, 0.868, 0.829, respectively. Ratio of minimal ADC showed the largest AUC. Logistic regression analysis was used to test the combination of DWI (ratio of minimal ADC + ratio of peritumoral ADC) parameters. A combination of ratio of minimal ADC and ratio of peritumoral ADC for the diagnosis of H3 K27M mutations showed the largest AUC of 0.872, resulting in sensitivity, specificity of 88.89%, 76.92%, respectively. The results of the ROC analysis are shown in Table 4, Fig. 6.

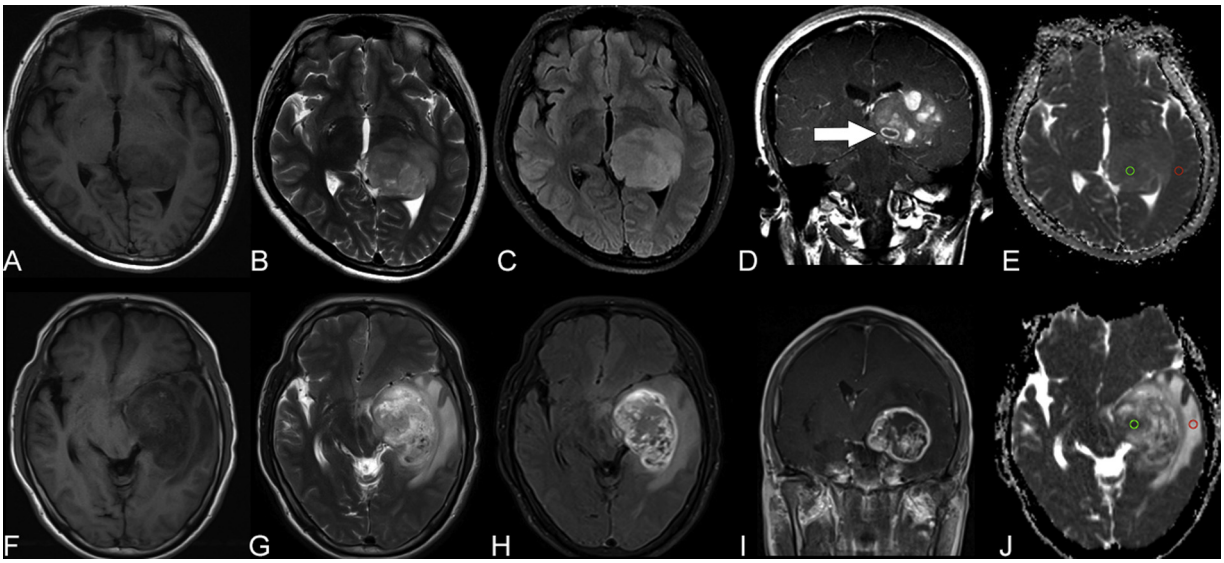

Fig. 2. T1WI (A, F), T2WI (B, G), flair (C, H), coronal contrast-enhancing (D, I), and selection of ROI on the ADC greyscale map (E, J) were obtained from 2 patients with gliomas located in the left thalamus. Upper images (A, B, C, D, E) demonstrate a H3 K27M-mutant glioma in a 35-year-old female. The H3 K27M-mutant glioma shows a heterogeneous mass with sharp borders, round or oval shape, absence of edema, and intratumoral nodular rim enhancement (*white arrow*). Lower images (F, G, H, I, J) demonstrate a H3 K27M wild-type glioma in a 42-year-old male: this glioma shows heterogeneous cystic mass with blurred borders, an round or oval shape, edema, and marginal enhancement. ROI of the tumor parenchyma (*green ring*) was placed in the lowest signal intensity on the ADC grayscale map (E, J); ROI of the peritumoral area(*red ring*) was placed within 1 cm of the tumor margin (E) or in the edema area (J).

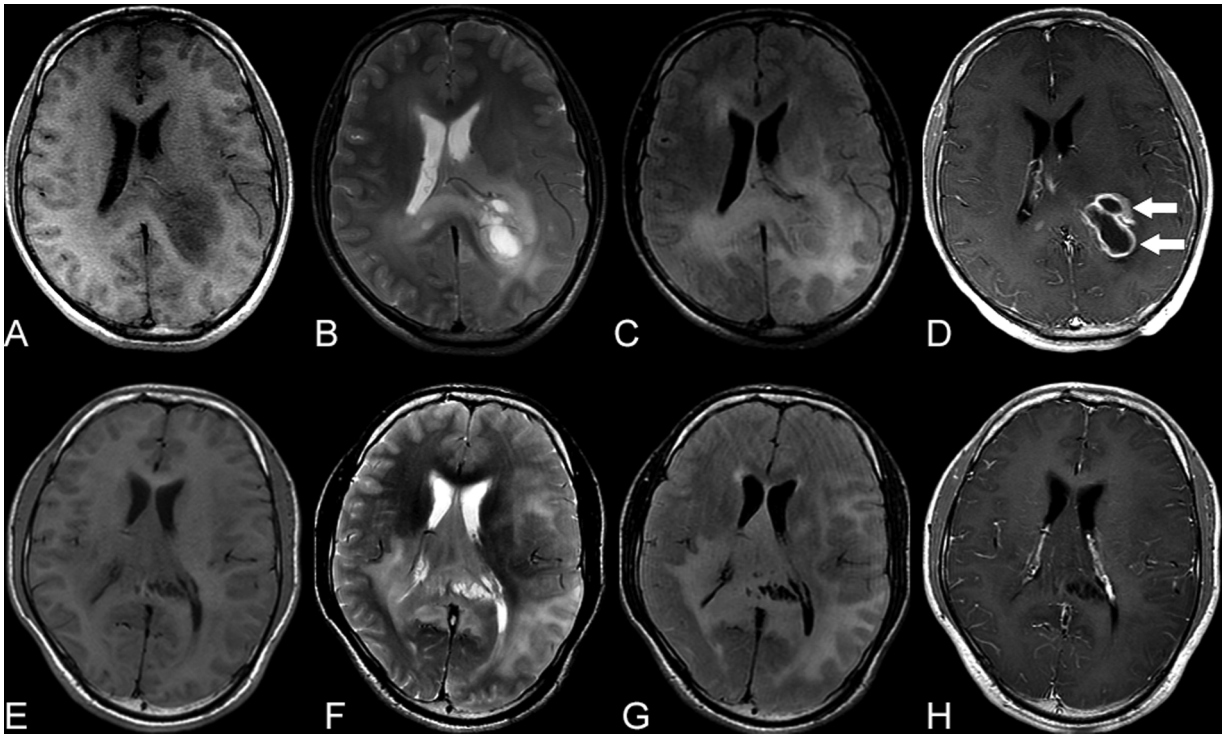

Fig. 3. Examples of H3 K27M-mutant (A, B, C, D) and H3 K27M wild-type (E, F, G, H) gliomas located in the corpus callosum. A 20-year-old male with H3 K27M-mutant glioma shows a heterogeneous cystic mass with blurred borders, irregular shape, edema, and intratumoral rim enhancement (*white arrow*). A 22-year-old male with H3 K27M wild-type glioma shows heterogeneous signal intensity with blurred margins, edema, and no or minimal enhancement.

4. Discussion

Our study demonstrated that minimal ADC ($\times 10^{-3}$ mm^2/s) with a threshold of 0.728, peritumoral ADC with a threshold of 1.004, ratio of minimal ADC with a threshold of 0.982, and ratio of peritumoral ADC with a threshold of 1.248 were significant independent variables for potentially predicting H3 K27M mutational status in diffuse midline gliomas. Combining DWI parameters of ratio of minimal and ratio of

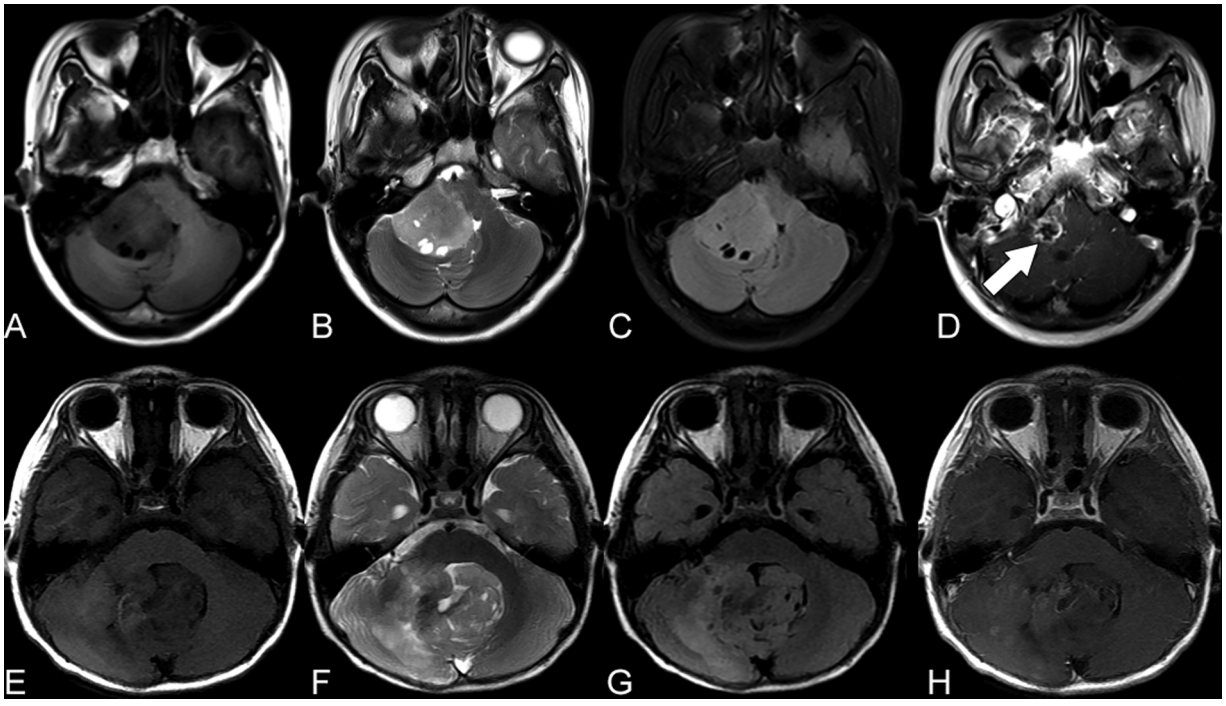

Fig. 4. Examples of H3 K27M-mutant (A, B, C, D) and H3 K27M wild-type (E, F, G, H) gliomas located in the cerebellum. A 24-year-old female with H3 K27M-mutant gliomas shows a heterogeneous cystic mass with sharp margins, hemorrhage, round or oval shape, and absence of edema. The upper part of the tumor shows intratumoral rim enhancement (*white arrow*). A 4-year-old male child with H3 K27M wild-type gliomas shows heterogeneous signal intensity, hemorrhage, blurred margins, slight edema, and no or minimal enhancement.

Table 3
Comparisons of ADC variables between H3 K27M-mutant and wild-type groups.

ADC ($\times 10^{-3}$ mm^2/s)	H3 K27M-mutant (n = 18)	H3 K27 M wild-type (n = 13)	*P* Value
minimal	0.734 ± 0.120	0.864 ± 0.112	0.020*
peritumoral	0.937 ± 0.156	1.161 ± 0.240	0.018*
internal capsule	0.759 ± 0.060	0.734 ± 0.039	0.378
ratio of minimal	0.972 ± 0.165	1.180 ± 0.162	0.018*
ratio of peritumoral	1.240 ± 0.232	1.582 ± 0.320	0.013*

* indicates statistical significance.

peritumoral ADC resulted in the largest AUC of 0.872, which could be considered reliable for predicting the H3 K27M mutational status. In addition, we found that patients with H3 K27M-mutant gliomas were significantly younger than those with H3 K27M wild-type gliomas. We also demonstrated that diffuse midline gliomas in different locations have diverse imaging features, it's challenging to identify H3 K27M mutational status solely depending on the cMRI manifestations.

Since the revised WHO edition of the classification of CNS tumors introduced molecular parameters to identify the concept of "H3 K27M-mutant diffusion midline gliomas" [1], most of the published literatures have focused on the pathology and clinical outcomes, and few studies have investigated the preoperative conventional and advanced MRI features of these tumors. Currently, the reference standard for testing the status of H3 K27M is DNA sequencing [23]. We retrospectively combined the ADC values as a noninvasive method to detect H3 K27M-mutant gliomas. The present study highlights the importance of using advanced MR imaging characteristics to detect H3 K27M-mutational status.

As observed in the present study, we found there were no distinguishing cMRI features between the H3 K27M-mutant gliomas and H3 K27M wild-type gliomas. Similarly, Aboian et al. [15] reviewed 24 H3 K27M-mutant patients and 9 H3 K27M wild-type patients and demonstrated that this disease had a diverse imaging appearance without distinguishing characteristics. As to the current knowledge, the current study of H3 K27M-mutant gliomas was not available to prove the relevance of cMRI features for clinical practice. Indeed, the cMRI features of H3 K27M-mutant gliomas needs to be further investigated by expanding the sample size, and the predictive value of cMRI in H3 K27M-mutant gliomas needs to be further studied.

In the current study, we demonstrated that the minimal ADC and ratio of minimal ADC of the H3 K27M-mutant gliomas was lower than that of the H3 K27 M wild-type gliomas. The minimum ADC value was thought to represent the highest cellularity and/or vascularity within heterogeneous tumors [13,24]. Previous studies have demonstrated that the minimal ADC values have been used to identify tumor grade and gene mutations [25–27]. Xing et al. [28] and Tan et al. [29] showed that minimum ADC and relative ADC were useful for predicting the IDH mutational status in astrocytoma. Javier [16] et al. found that lower ADC values were associated with IDH wild-type grade II diffuse gliomas and drive poor clinical outcomes. In our study, we showed that the minimal ADC value of the tumor parenchyma of the H3 K27M-mutant glioma was significantly lower than that of the wild-type group. Previous studies have shown that H3 K27M-mutant gliomas were associated with a poorer prognosis than H3 K27M wild-type gliomas [5,6,30]. Lober et al. demonstrated that lower ADC values can predict aggressive clinical behavior in pediatric patients with diffuse intrinsic

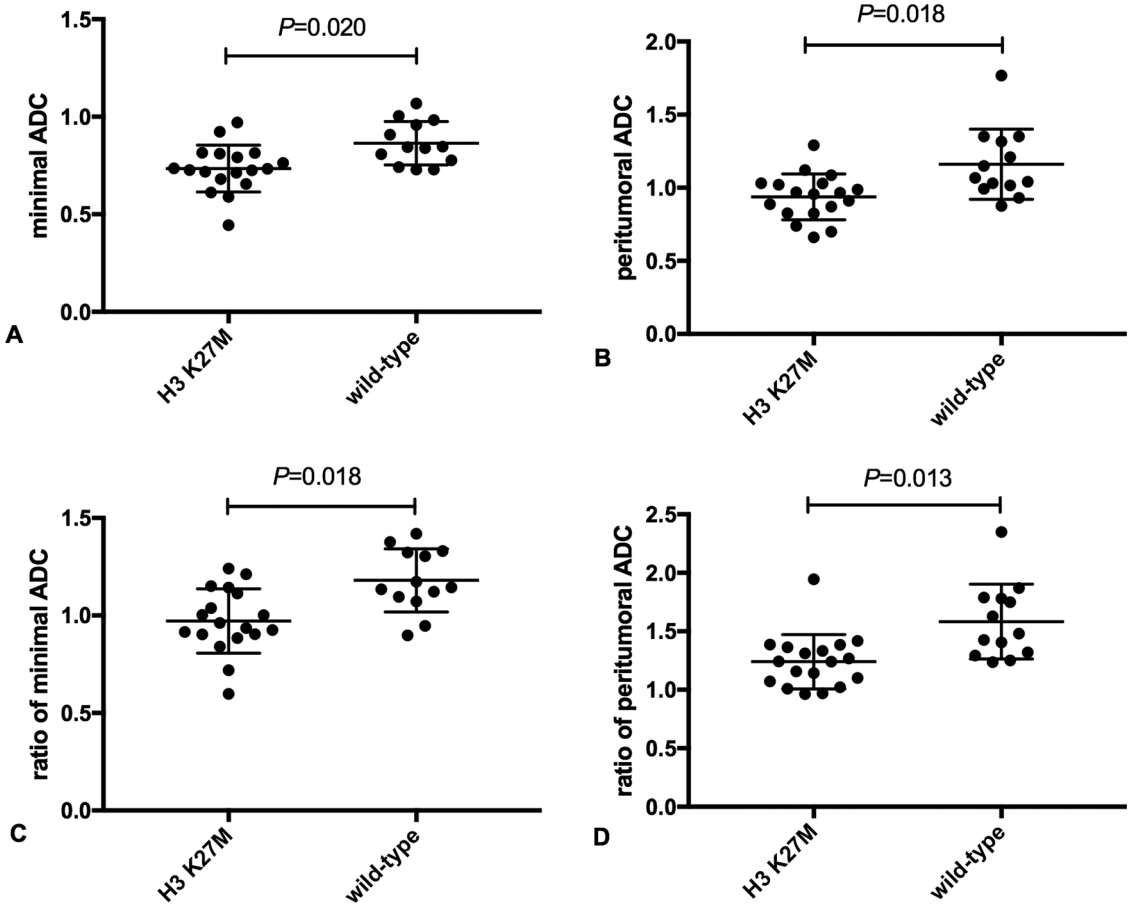

Fig. 5. Comparisons of ADC (unit: $\times 10^{-3}$ mm^2/s) variables between H3 K27M-mutant and wild-type groups. (A) The minimal ADC values ($P = 0.020$), (B) peritumoral ADC values ($P = 0.018$), (C) ratio of minimal ADC ($P = 0.018$), and (D) ratio of peritumoral ADC ($P = 0.013$) were significantly lower in the H3 K27M-mutant group than the H3 K27M wild-type group.

Table 4
Measurement of cut-off, sensitivity, specificity, and AUC of DWI parameters for assessing the H3 K27M status.

	Cut off	Sensitivity (%)	Specificity (%)	YI	AUC (95%CI)
Minimal ADC	0.728	94.44	61.54	0.56	0.842 (0.70-0.99)
Peritumoral ADC	1.004	66.67	84.61	0.51	0.806 (0.65-0.96)
Ratio of minimal ADC	0.982	88.89	76.92	0.66	0.868 (0.73-1.00)
Ratio of peritumoral ADC	1.248	88.89	69.23	0.58	0.829 (0.68-0.97)
Combination of DWI parameters	–	88.89	76.92	0.66	0.872 (0.75-1.00)

YI, Youden index; AUC, area under the curve. Combination of DWI parameters = ratio of minimal ADC + ratio of peritumoral ADC.

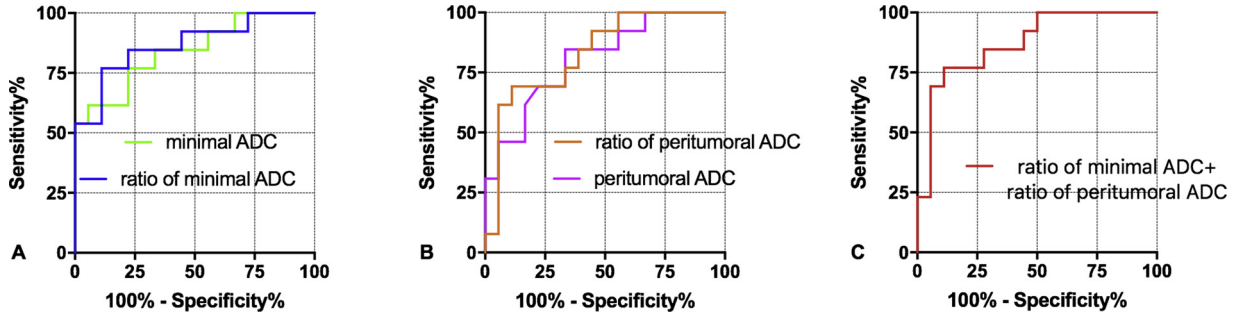

Fig. 6. ROCs with statistical significance were observed in H3 K27M-mutant gliomas. (A) The AUCs of the minimal ADC and ratio of minimal ADC were 0.84 and 0.87, respectively. (B) The AUCs of peritumoral ADC and ratio of peritumoral ADC were 0.81 and 0.83, respectively. (C) The AUC of the combination of DWI parameters (ratio of minimal ADC + ratio of peritumoral ADC) was 0.872. A combination of DWI parameters showed the largest AUC.

pontine glioma [31]. The lower ADC values in the H3 K27M-mutant group may be interpreted by the glial differentiation within the H3 K27M-mutant tumor [32]. The complicated polygene-associated process of tumorigenesis in glioma may be another reason for this result [6,33].

Moreover, we found that the peritumoral area within the H3 K27M-mutatnt gliomas also showed lower ADC values, indicating higher cell density adjoining to the tumor area. A previous study showed that the ADC value of vasogenic edema was higher than that of the peritumoral area infiltrated by tumor cells [34]. Castel et al. demonstrated that compared with H3.1, the more aggressive H3.3 tumors showed less extensive extracellular edema [3]. Previous studies have demonstrated that the ion channels of invading glioma cells and the role of the cell adhesion molecules may disrupt brain function [35,36].

Besides, we found that patients with H3 K27M mutations were 15 years younger than H3 K27M wild-type patients. Although H3 K27M-mutant midline diffuse gliomas predominately affect children and adolescents, they can also occur in adults [37,38]. Wang et al. showed that compared with adults, there was no statistical tendency of a poorer overall survival (OS) in children [9]. Furthermore, we demonstrated that one-half cases of the diffuse midline gliomas carried the H3 K27M mutation. The probability of H3 K27M mutation is consistent with previous reports [18,30].

Our study has several limitations. First, this was a retrospectively review from a single institution, and the tumor size was relatively small. A prospective investigation with a larger sample size is needed to verify these results. Second, the clinical outcomes were not available because of the irregular and short-term follow-up period. Third, we did not subgroup the histone of H3.3/H3.1, and the TP53, MGMT and IDH status was not reviewed in our study. Because of low incidence of the H3 K27M-mutant gliomas, the sample size was inadequate, and there are already several other studies that have investigated the other gene status in H3 K27M-mutant gliomas [2,32]. Fourth, the ADC values were obtained from multiple parametric MR protocols, which may reduce the feasibility of quantitative analysis.

5. Conclusion

Compared with H3 K27M wild-type midline gliomas, the H3 K27M-mutant midline gliomas had lower minimum ADC values in the solid parts and peritumoral area. The minimal ADC with a threshold of 0.728, peritumoral ADC with a threshold of 1.004, ratio of minimal ADC with a threshold of 0.982, and ratio of peritumoral ADC with a threshold of 1.248 were imaging predictors of H3 K27M mutations. A combination of ADC values in the solid parts and peritumoral area may provide a more accurate predictor to detect the H3 K27M mutational status in midline gliomas of the brain. However, due to the small size of our study, a larger sample size study is necessary.

Conflict of interest statement

Authors have no conflict of interest to disclose.

Funding

This research did not receive any specific grant from funding agencies in the public, commercial, or not-for-profit sectors.

References

[1] D.N. Louis, A. Perry, G. Reifenberger, et al., The 2016 world health organization classification of tumors of the central nervous system: a summary, Acta Neuropathol. 131 (2016) 803–820, https://doi.org/10.1007/s00401-016-1545-1.
[2] D.A. Solomon, M.D. Wood, T. Tihan, et al., Diffuse midline gliomas with histone H3-K27M mutation: a series of 47 cases assessing the Spectrum of morphologic variation and associated genetic alterations, Brain Pathol. 26 (2016) 569–580, https://doi.org/10.1111/bpa.12336.
[3] D. Castel, C. Philippe, R. Calmon, et al., Histone H3F3A and HIST1H3B K27M mutations define two subgroups of diffuse intrinsic pontine gliomas with different prognosis and phenotypes, Acta Neuropathol. 130 (2015) 815–827, https://doi.org/10.1007/s00401-015-1478-0.
[4] G. Wu, A. Broniscer, T.A. McEachron, et al., Somatic histone H3 alterations in pediatric diffuse intrinsic pontine gliomas and non-brainstem glioblastomas, Nat. Genet. 44 (2012) 251–253, https://doi.org/10.1038/ng.1102.
[5] K. Aihara, A. Mukasa, K. Gotoh, et al., H3F3A K27M mutations in thalamic gliomas from young adult patients, Neuro Oncol. 16 (2014) 140–146, https://doi.org/10.1093/neuonc/not144.
[6] D. Meyronet, M. Esteban-Mader, C. Bonnet, et al., Characteristics of H3 K27M-mutant gliomas in adults, Neuro Oncol. 19 (2017) 1127–1134, https://doi.org/10.1093/neuonc/now274.
[7] M. Gessi, G.H. Gielen, V. Dreschmann, et al., High frequency of H3F3A (K27M) mutations characterizes pediatric and adult high-grade gliomas of the spinal cord, Acta Neuropathol. 130 (435) (2015), https://doi.org/10.1007/s00401-015-1463-7.

[8] J. Schwartzentruber, A. Korshunov, X.Y. Liu, et al., Driver mutations in histone H3.3 and chromatin remodelling genes in paediatric glioblastoma, Nature 482 (2012) 226–231, https://doi.org/10.1038/nature10833.
[9] L. Wang, Z. Li, M. Zhang, et al., H3 K27 M-mutant diffuse midline gliomas in different anatomical locations, Hum. Pathol. (2018), https://doi.org/10.1016/j.humpath.2018.04.015.
[10] Y.J. Heo, J.E. Park, H.S. Kim, et al., Prognostic relevance of gemistocytic grade II astrocytoma: gemistocytic component and MR imaging features compared to non-gemistocytic grade II astrocytoma, Eur. Radiol. 27 (2017) 3022–3032, https://doi.org/10.1007/s00330-016-4649-z.
[11] Y. Cui, L. Ma, X. Chen, et al., Lower apparent diffusion coefficients indicate distinct prognosis in low-grade and high-grade glioma, J. Neurooncol. 119 (2014) 377–385, https://doi.org/10.1007/s11060-014-1490-6.
[12] S.C. Thust, S. Hassanein, S. Bisdas, et al., Apparent diffusion coefficient for molecular subtyping of non-gadolinium-enhancing WHO grade II/III glioma: volumetric segmentation versus two-dimensional region of interest analysis, Eur. Radiol. 28 (2018) 3779–3788, https://doi.org/10.1007/s00330-018-5351-0.
[13] D.M. Patterson, A.R. Padhani, D.J. Collins, Technology insight: water diffusion MRI–a potential new biomarker of response to cancer therapy, Nat. Clin. Pract. Oncol. 5 (2008) 220–233, https://doi.org/10.1038/ncponc1073.
[14] S. Lee, S.H. Choi, I. Ryoo, et al., Evaluation of the microenvironmental heterogeneity in high-grade gliomas with IDH1/2 gene mutation using histogram analysis of diffusion-weighted imaging and dynamic-susceptibility contrast perfusion imaging, J. Neurooncol. 121 (2015) 141–150, https://doi.org/10.1007/s11060-014-1614-z.
[15] M.S. Aboian, D.A. Solomon, E. Felton, et al., Imaging characteristics of pediatric diffuse midline gliomas with histone H3 K27M mutation, AJNR Am. J. Neuroradiol. 38 (2017) 795–800, https://doi.org/10.3174/ajnr.A5076.
[16] J.E. Villanueva-Meyer, M.D. Wood, B.S. Choi, et al., MRI features and IDH mutational status of grade II diffuse gliomas: impact on diagnosis and prognosis, AJR Am. J. Roentgenol. 210 (2018) 621–628, https://doi.org/10.2214/AJR.17.18457.
[17] D. Bechet, G.G. Gielen, A. Korshunov, et al., Specific detection of methionine 27 mutation in histone 3 variants (H3K27M) in fixed tissue from high-grade astrocytomas, Acta Neuropathol. 128 (2014) 733–741, https://doi.org/10.1007/s00401-014-1337-4.
[18] P. Buczkowicz, U. Bartels, E. Bouffet, et al., Histopathological spectrum of paediatric diffuse intrinsic pontine glioma: diagnostic and therapeutic implications, Acta Neuropathol. 128 (2014) 573–581, https://doi.org/10.1007/s00401-014-1319-6.
[19] I.S. Khayal, S.R. Vandenberg, K.J. Smith, et al., MRI apparent diffusion coefficient reflects histopathologic subtype, axonal disruption, and tumor fraction in diffuse-type grade II gliomas, Neuro-Oncology 13 (2011) 1192–1201.
[20] A. Brander, A. Kataja, A. Saastamoinen, et al., Diffusion tensor imaging of the brain in a healthy adult population: normative values and measurement reproducibility at 3 T and 1.5 T, Acta Radiol. 51 (2010) 800–807, https://doi.org/10.3109/02841851.2010.495351.
[21] J. Xiong, W. Tan, J. Wen, et al., Combination of diffusion tensor imaging and conventional MRI correlates with isocitrate dehydrogenase 1/2 mutations but not 1p/19q genotyping in oligodendroglial tumours, Eur. Radiol. 26 (2016) 1–11, https://doi.org/10.1007/s00330-015-4025-4.
[22] M.J. O'Donnell, S.L. Chin, S. Rangarajan, et al., Global and regional effects of potentially modifiable risk factors associated with acute stroke in 32 countries (INTERSTROKE): a case-control study, Lancet 388 (2016) 761–775.
[23] D. Sturm, H. Witt, V. Hovestadt, et al., Hotspot mutations in H3F3A and IDH1 define distinct epigenetic and biological subgroups of glioblastoma, Cancer Cell 22 (2012) 425–437, https://doi.org/10.1016/j.ccr.2012.08.024.
[24] P.D. Humphries, N.J. Sebire, M.J. Siegel, et al., Tumors in pediatric patients at diffusion-weighted MR imaging: apparent diffusion coefficient and tumor cellularity, Radiology 245 (2007) 848, https://doi.org/10.1148/radiol.2452061535.
[25] E.J. Lee, S.K. Lee, R. Agid, et al., Preoperative grading of presumptive low-grade astrocytomas on MR imaging: diagnostic value of minimum apparent diffusion coefficient, AJNR Am. J. Neuroradiol. 29 (2008) 1872–1877, https://doi.org/10.3174/ajnr.A1254.
[26] C.H. Suh, H.S. Kim, S.C. Jung, et al., Diffusion-weighted imaging and diffusion tensor imaging for differentiating high-grade glioma from solitary brain metastasis: a systematic review and meta-analysis, AJNR Am. J. Neuroradiol. 39 (2018) 1208–1214, https://doi.org/10.3174/ajnr.A5650.
[27] R. Murakami, T. Hirai, T. Sugahara, et al., Grading astrocytic tumors by using apparent diffusion coefficient parameters: superiority of a one- versus two-parameter pilot method, Radiology 251 (2009) 838–845, https://doi.org/10.1148/radiol.2513080899.
[28] Z. Xing, X. Yang, D. She, et al., Noninvasive assessment of IDH mutational status in world health organization grade II and III astrocytomas using DWI and DSC-PWI combined with conventional MR imaging, AJNR Am. J. Neuroradiol. 38 (2017), https://doi.org/10.3174/ajnr.A5171.
[29] W.L. Tan, W.Y. Huang, B. Yin, et al., Can diffusion tensor imaging noninvasively detect IDH1 gene mutations in astrogliomas? A retrospective study of 112 cases, AJNR Am. J. Neuroradiol. 35 (2014) 920, https://doi.org/10.3174/ajnr.A3803.
[30] J. Feng, S. Hao, C. Pan, et al., The H3.3 K27M mutation results in a poorer prognosis in brainstem gliomas than thalamic gliomas in adults, Hum. Pathol. 46 (2015) 1626–1632, https://doi.org/10.1016/j.humpath.2015.07.002.
[31] R.M. Lober, Y.J. Cho, Y. Tang, et al., Diffusion-weighted MRI derived apparent diffusion coefficient identifies prognostically distinct subgroups of pediatric diffuse intrinsic pontine glioma, J. Neurooncol. 117 (2014) 175–182, https://doi.org/10.1007/s11060-014-1375-8.
[32] D.A. Khuong-Quang, P. Buczkowicz, P. Rakopoulos, et al., K27M mutation in histone H3.3 defines clinically and biologically distinct subgroups of pediatric diffuse intrinsic pontine gliomas, Acta Neuropathol. 124 (2012) 439–447, https://doi.org/10.1007/s00401-012-0998-0.
[33] C. Jones, S.J. Baker, Unique genetic and epigenetic mechanisms driving paediatric diffuse high-grade glioma, Nat. Rev. Cancer 14 (2014) 651–661, https://doi.org/10.1038/nrc3811.
[34] G. Pavlisa, M. Rados, G. Pavlisa, et al., The differences of water diffusion between brain tissue infiltrated by tumor and peritumoral vasogenic edema, Clin. Imaging 33 (2009) 96–101, https://doi.org/10.1016/j.clinimag.2008.06.035.
[35] V.A. Cuddapah, S. Robel, S. Watkins, et al., A neurocentric perspective on glioma invasion, Nat. Rev. Neurosci. 15 (2014) 455–465, https://doi.org/10.1038/nrn3765.
[36] W.C. Wai, D.E. Dye, D.R. Coombe, The role of immunoglobulin superfamily cell adhesion molecules in cancer metastasis, Int. J. Cell Biol. (2012) 340296, , https://doi.org/10.1155/2012/340296 2012.
[37] M. Karremann, G.H. Gielen, M. Hoffmann, et al., Diffuse high-grade gliomas with H3 K27M mutations carry a dismal prognosis independent of tumor location, Neuro Oncol. 20 (2017), https://doi.org/10.1093/neuonc/nox149.
[38] G. Reyes-Botero, M. Giry, K. Mokhtari, et al., Molecular analysis of diffuse intrinsic brainstem gliomas in adults, J. Neurooncol. 116 (2014) 405–411, https://doi.org/10.1007/s11060-013-1312-2.